Dynamic loads arising from broken wave impacts on a cylindrical turbine substructure in shallow waters

Davide Banfi, Alison Raby, and David Simmonds

Abstract—**The market of tidal and wind turbines has significantly grown in recent years. Although monopile substructures are usually the preferred option, the use of the so-called Gravity Base Foundations is still needed at sites where installation of piles is difficult. Because Gravity Base Foundations are typically located in shallow water depths, such structures can be exposed to the load caused by broken waves. Currently, the wave load due to broken impacts on cylindrical structures is estimated according to the Morison equation. However, such formulation does not allow evaluating the dynamic response of the structure as the load impact duration is not explicitly taken into account.**

The aim of this paper is to analyse the dynamic load due to broken waves obtained from a small-scale cylindrical model in a limited depth condition.

Results obtained by means of load cell measurements show that dimensionless force peaks have a tendency to decrease as the dimensionless impact duration increases. When compared to the Morison equation, the maximum measured force was found to be 36% underestimated. A dimensionless formula is proposed to calculate the rise time and the force peak by means of four variables: breaking wave height, water depth, wave period and diameter.

Keywords—**Broken waves, cylindrical structure, dynamic load, Gravity Base Foundations, laboratory test, shallow waters, turbine substructures.**

I. Introduction

GLOBAL warming and a fossil fuel shortage have led to an increased use of renewable energies in recent years [1]-[2]-[3]-[4]. Among the technologies being used, tidal and offshore wind energy have made significant progress, with a growing number of turbines being deployed and grid-connected worldwide [5]-[6]. In this context, turbine support structures can be categorized into different types depending on their configuration, which is generally identified on the basis of the site characteristics i.e. water depth and geotechnical properties of the seabed [7]-[8]-[9]. The sea depth is the most important factor for the viability of offshore wind farms because the cost for foundations significantly increases with depth [10]. As illustrated in Fig. 1, four main support structure types can be distinguished on the basis of the water depth:

- Gravity Base Foundations (GBFs);
- Monopiles;
- Jacket/tripod structures;
- Floating structures.

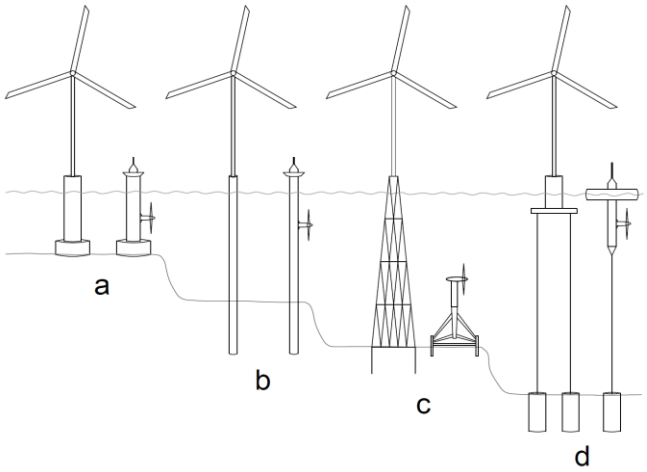

Fig. 1. Different turbine support structures distinguished on the basis of the water depth: (a) Gravity Base Foundations, (b) Monopiles, (c) Jacket/tripod, (d) Floating structures.

The first commercial-scale and grid-connected tidal turbine (SeaGen, UK) was installed in 2008. This turbine has two rotors mounted at the outer ends of a pair of streamlined wing-like arms. These are supported by a monopile foundation that extends 9 m above the average sea level for safe and easy maintenance access [11]. The installation of tidal turbine substructures has indirectly gained expertise from the market of offshore wind

13th EWTEC 2019: European Wave and Tidal Energy Conference. ID paper number: 1545. Section: Station-keeping, moorings and foundations.

D. Banfi was a PhD researcher at Plymouth University, School of Engineering, Plymouth, UK. He is now working in the private sector for JBA Consulting (Coastal and Maritime Engineering) as a Coastal Engineer (e-mail: davide.banfi@plymouth.ac.uk).

A. Raby is Full Professor in Coastal Engineering at Plymouth University, School of Engineering, Drake Circus, Plymouth, PL4 8AA, UK (e-mail: alison.raby @plymouth.ac.uk).

D. Simmonds is Associate Professor in Coastal Engineering at Plymouth University, School of Engineering, Drake Circus, Plymouth, PL4 8AA, UK (e-mail: d.simmonds@plymouth.ac.uk).

turbines, as the first wind farm was installed in 1991 (Vindeby, Denemark) [12] – monopiles (76%) and GBFs (12%) dominate the European market of offshore wind turbine foundations [13].

A monopile is a single large-diameter steel tube that penetrates into the seabed. Existing offshore monopiles are typically 3-7.5 m in diameter and they have been used in water depths up to 30 m [14].

Gravity based foundations (GBFs) gain their stability solely by means of their own weight and they are thus characterized by larger diameters with respect to the monopiles. GBFs are typically concrete shell structures and the ballast required to obtain sufficient gravity consists of water, sand/rock or concrete that is filled into the structure [15]. So far, they have demonstrated to be technically feasible and economically viable in shallow water conditions. The first GBFs for offshore wind turbines were installed in Denmark in 1991, in a water depth of 5 m [16]. Afterwards, several GBF types have been typically installed in shallow waters ranging from 2 m to 15 m [17]. Among them, circular base foundations are usually preferred over rectangular foundations as they have a minor overall scour erosion [18], which is further less significant when the gravity base foundation has a flat-topped transition rather than a conical shape [19].

The construction costs of GBFs are usually cheaper when compared to those of monopiles as steel is 7-8 times more expensive than the concrete [20]. However, the offshore wind turbine market is dominated by monopile foundations as installation costs tend to be lower for them. This is given by the fact that for monopiles the installation technique is derived from the offshore oil and gas industry, where there is a lot of experience with the use of steel tubular foundations. Consequently, offshore equipment needed for drilling the monopiles into the seabed is widely available, allowing thus a decrease of installation costs [20]. Monopile foundations are usually, therefore, the preferred option as they have also been proven to be structurally reliable over the time.

Although monopiles are typically the preferred option, the use of GBFs is still needed at sites where installation of piles in the underlying seabed is difficult, such as at tidal and wind farm sites located on a hard rock ledge [8]. In this regard, the wave load is typically estimated according to Morison equation [21], at least in first instance. However, GBFs can be exposed to the load caused by broken waves due to the limited water depth. In such condition, Morison equation, which has been developed on the basis of non-breaking waves on slender cylinders, cannot be properly used to evaluate the dynamic load on the structure [22]. The dynamic assessment for the cylindrical substructure is a crucial aspect of the design process as they are long slender members supporting a significant mass (rotor and nacelle) that amplify the structural response of the foundation. Therefore, their dynamic characteristics are completely different from those typical of fixed oil and gas structures [8]. Consequently, it is design practise to assess the dynamic response of turbine substructures on the basis of different wave impulses as they lead to different structural responses. In this regard, several investigations have already highlighted that dynamic analyses should be carefully carried out as the impulse and the impact duration play a key role in the structural response [23]-[24].

In this paper, the effects of the limited water depth on the dynamic load due to broken waves are illustrated by comparing laboratory results with the Morison equation. Such analyses arise from an in-depth field and laboratory small-scale tests on the Eddystone lighthouse (UK). This is a rock lighthouse exposed to this type of impact due to the limited depth conditions.

II. Wave load on Cylindrical structures

A. *Quasi-static load and Morison equation*

Wave loads are typically classified into three categories, namely: non-breaking, breaking and broken waves.

The wave is non-breaking when the wave height (H) is much smaller with respect to the water depth (h). In this case, the wave load is in phase with the wave surface elevation (quasi-static load). Therefore, the maximum pressure head is about the incident wave height and the time rise (tr) – time taken to get to the peak load from 0 – is a quarter of the wave period (0.25T).

The breaking occurs when the individual wave exceeds the wave steepness limit ($H/L \simeq 0.14$) or the wave height limit ($H/h \simeq 1$) – where L is the wavelength.

In deep-intermediate water, the primary cause for wave breaking is due to the wave steepness limit [22]. The wave crest becomes unstable and cascades down producing a foamy water surface. This breaker is called spilling and it is a weak form of breaking as the wave gradually and slowly dissipates its energy [25].

During the propagation from deep to shallow waters, the wavelength (L) decreases and the wave height (H) tends to increase until that $H/h \simeq 1$ [22]. The wave steepness can quickly increase, especially when it propagates on steep slopes [26]. In this case, the crest curls over the shoreward face of the wave, inducing so a water jet [25]. This is a plunging breaker and it is a violent form of breaking that generates an impulsive load if the water jet hits the structure – a load is defined impulsive when it is characterized by an extreme peak with a short impact duration.

The wave is then called broken when the plunging jet splashes into the water. In this case, the structure is hit by a turbulent bore. Two load peaks can usually be detected for a broken wave. The first peak, which corresponds to the impact of the foamy bore, tends to be higher [27]. The subsequent peak tends to be in phase with the wave period. Although broken waves are characterized by lower load peaks when compared to plunging impacts, the turbulent bore can have a relatively high residual velocity that can cause a more impulsive load with respect to non-

breaking or spilling waves [28]-[29]. In this regard, field measurements obtained by geophones installed on the Eddystone lighthouse include relatively large structural oscillations caused by broken impacts. In contrast, no displacements have been recorded for non-breaking waves due to the limited depth condition, which causes the breaking of larger waves farther from the lighthouse [24].

Generally, offshore monopiles in deep-intermediate waters are exposed to the load caused by non-breaking or spilling waves. In such condition, the wave load is normally estimated on the basis of Morison equation [21]-[22]. In this formulation, the horizontal force on a vertical element dz of the structure at level z is given by the as the sum of the quasi-static drag F_D and inertia force F_I, as illustrated below:

$$dF = dF_D + dF_I \tag{1}$$

$$dF_D = 0.5\,\rho\,C_D\,D\,u\,|u|\,dz \tag{2}$$

$$dF_I = 0.25\,\pi\,\rho\,C_M\,D^2\,\dot{u}\,dz \tag{3}$$

where ρ is the mass density of water, D is the pile diameter, u is the water particle velocity, $\dot{u}$ is the water particle acceleration, C_D and C_M are empirical coefficients called drag and inertia coefficient, respectively.

Morison formulated his equation simply by hypothesizing that the superposition of two separate phenomena i.e. drag in a current and hydrodynamic inertia in an accelerating flow. Therefore, the drag is the resistance force of the structure to the wave motion; while the inertia is the force on the structure due to the acceleration change of the wave during the propagation.

B. Water velocity particles and applications in shallow waters

Velocities and accelerations need to be integrated in space and time to determine the force time history acting over the cylinder. The wave theory shall be selected with due consideration of the water depth and of the range of validity of the theory.

In deep-intermediate waters, the particle velocities and accelerations can be estimated by means of the linear theory of Airy (small wave amplitude). The horizontal velocity and acceleration under the wave at the centerline (x=0) of the cylinder for Airy theory are shown below.

$$u\,(z,t) = \frac{\pi\,H}{T}\,\frac{cosh\,[k\,(z+h)]}{sinh\,(kh)}\,\cos\left(\frac{2\,\pi\,t}{T}\right) \tag{4}$$

$$\dot{u}\,(z,t) = \frac{2\pi^2\,H}{T^2}\,\frac{cosh\,[k\,(z+h)]}{sinh\,(kh)}\,\sin\left(\frac{2\,\pi\,t}{T}\right) \tag{5}$$

As may be observed from (4) and (5), the velocity and the acceleration are out of phase of 90°. Thus, when F_D is maximum F_I is 0 and vice versa.

The linear theory ignores contributions to the force from the wave crest above the still water level at z=0 (integration from –h to 0). This is a minor problem when the inertia force F_I is the dominating component. If the drag force F_D is the dominating component, a significant error can be introduced by ignoring the contribution from the wave crest [22].

For long waves in shallow water, the water particle velocity tends to be constant over the depth. In this case, it is usually recommended to use the maximum horizontal water particle velocity (u_{MAX}) extended at the free surface [22]. However, linear wave theory should be used with caution [30], since it may not always be adequate to predict wave forces [31], especially when waves propagate on steep slopes [32]. In such conditions, the wave tends to be asymmetric and several investigations have found that both the wave force and the wave celerity tend to increase [26]. Consequently, in shallow water situations it is a usual design practice to set the velocity of the water particle (u_{MAX}) equal to the wave celerity (C_b=L_b/T) at the breaking point [33]. This assumption derives from the fact that the breaking starts when the velocity of the particle in the crest equals the celerity of the wave. Since at breaking point the wave height and the water depth have similar size ($H_b \simeq h_b \simeq 1$), two similar expressions are usually applied to simplify the wave force estimation, as illustrated below.

$$C_b = \frac{L_b}{T} \approx \sqrt{g\,h_b} \approx \sqrt{g\,H_b} \tag{6}$$

C. Drag and Inertia coefficients

The coefficients C_D and C_M can be empirically determined by means of laboratory experiments, taking advantage of the fact that the two components are out of phase of 90°. Thus, the particle acceleration $\dot{u}$ is 0 at wave crest or trough and C_D can be determined. As the wave passes the cylinder (nodal line at the still water), the particle velocity u is 0 and C_M can thus be determined.

Multiple studies have carried out laboratory experiments in order to estimate the values of the inertia and the drag coefficients [34]. These have been found to be dependent on Keulegan-Carpenter number (KC=u_{MAX}T/D), Reynolds number (Re=u_{MAX}D/ν) and roughness parameters – where u_{MAX} is the maximum horizontal particle velocity at the still water level and ν is the kinematic viscosity of seawater. In design situations, the drag and the inertia coefficients are typically in the in the ranges $0.6 < C_D < 1.2$ and $1.5 < C_M < 2.0$, respectively [22].

D. Relative importance of Drag versus Inertial Force terms

Understanding the maximum forces and also when inertial effects dominate over viscous drag, or vice versa, can significantly simplify the force estimation.

Morison found that the relative importance of the inertial force decreases for shallow waters (h/L small) or for large waves with respect to the structure (H/D large) [35]. In this regard, the Keulegan-Carpenter number is a

well-established indicator used to evaluate the relative importance of drag versus inertia forces for a given situation.

The relative component importance can be analysed by comparing the magnitude amplitudes of the drag and inertia forces, as shown in (7) – note that the ±90° phase difference between the force components is completely neglected.

$$\frac{\overline{F_D}}{\overline{F_I}} = \frac{1/2\ (\rho\ C_D\ D\ \bar{u}\ |\bar{u}|)}{\pi/4\ (\rho\ C_M\ D^2\ \bar{u}\ 2\pi/T)} \approx \frac{1}{10}\frac{C_D}{C_M} KC \tag{7}$$

As can be observed from (7), the drag and inertia amplitudes are equal when KC is approximately 10. Due to the fact that the two components are out of phase, in design situations the drag force is neglected when KC ≤ 5 as the flow theory is still applicable. Both components are considered when 5 < KC ≤ 15. The inertia component is generally neglected when KC > 15 as the vortex shedding frequency becomes high compared to the wave frequency [36]. Thus, the water flow tends to behave more and more like a uniform flow. Indeed, the flow corresponds to a constant current when KC tends to infinite.

E. Assumptions and limitations

Morison equation can be used to estimate the force for the portion of the cylinder that is submerged. Such formulation is generally valid for non-breaking waves on slender cylinders that do not considerably modify the incident waves i.e. when the ratio *D*/L is lower than 0.2. Alternatively, the force estimation should take into account the diffraction theory. However, this cannot be applied when waves are fully broken.

As the formulation was developed on the basis of non-breaking waves, force components due to breaking run-ups are not considered [22]. In this regard, the rock lighthouse investigation has shown that broken impacts can lead to roughly uniform spatial distributions with application points of the overall force above the still water level [24].

In dynamic analyses, the load time history is assumed to be in phase with the wave surface elevation. However, the load time history depends on the type of breaking [37]-[38]. Therefore, appropriate considerations should be taken into account when waves are likely to break on the site of the structure (plunging impacts) or in its vicinity (broken impacts) [22].

F. Slamming force caused by a plunging jet

For plunging impacts, a further slamming force needs to be considered during the design process [22]-[37]-[39]. This shock load, which is caused by the plunging jet hitting the cylinder, is usually estimated according to the formulation provided by Wienke & Oumeraci [22]-[40]. Their model assumes a shock impulse that is added on the top of the quasi-static force of Morison. Therefore, the total force on the cylinder at the peak instant is expressed as below.

$$F_{TOT} = F_D + F_I + F_S \tag{8}$$

The slamming force is typically expressed in the form of the drag component of Morison, as follows:

$$F_D = 0.5\ \rho\ C_S\ D\ u^2\ \Delta z \tag{9}$$

where C_S is called slamming coefficient and it is set equal to 2π according to the model proposed by Wienke & Oumeraci [40]. The impact extent Δz has been empirically related to the breaking wave height (H_b) by means of the so-called curling factor (λ_F), which is set at 0.46 for plunging impacts breaking immediately in front of a vertical cylinder. As in shallow water situations the wave surface elevation (η_b) is asymmetric i.e. $\eta_b = 0.78 H_b$, the impact extent results to be equal to $\Delta z = \lambda_F\ \eta_b = 0.46\ 0.78\ H_b$; while the water particle velocity is set equal to the wave celerity at breaking i.e. $u = C_b$ [22]-[40]. The slamming force is characterized by a very short impact duration. Wienke & Oumeraci used pressure transducers installed around the cylinder in order to estimate the time taken by the water jet to submerge half section of the cylinder. Due to the so-called pile-up effect, their model assumes an impact duration equal to $0.20u/D$ [40]. Recently, an alternative formulation has been provided by Paulsen et al. [41], who determine the impact duration on the basis of the wave period.

It should be noted that Wienke & Oumeraci's model provides the wave force for the critical load condition i.e. when the plunging waves breaks just in front of the vertical cylinder. With increasing breaking distances, the force peak decreases and the impact durations increases [28]-[40]. However, while multiple investigations have analysed the wave load on cylindrical structures due to non-breaking (seawards of surf zone) and breaking waves (surf zone), broken waves – turbulent bores that occur at the shoreward of surf zone (i.e. in limited water depths) – have received a minor attention so far.

III. METHODOLOGY

Regular wave tests were conducted to investigate how the wave load on a cylindrical structure is affected by limited depth conditions.

The experiments were carried out in the 35 m long x 0.6 m wide x 1.2 m deep sediment wave flume of the Coast Laboratory at Plymouth University.

The test program was designed to generate a comprehensive data set covering a broader range of wave conditions, including also waves that break farther from the structure i.e. broken impacts. To this aim, 128 runs of regular waves were generated with target values of H_o and T comprised between 0.02-0.25 m and 0.6-3.0 s, respectively.

The model comprised two circular cylinders (one above the other) having different diameters (0.2 and 0.15 m) with a flat-topped transition just 0.01 m above the still water

level. Such geometrical configuration has been commonly adopted in the design of masonry rock lighthouses in order to reduce the wave run up by breaking the vertical water motion [42], which is a crucial aspect in the design of offshore wind turbine [43]-[44]. The water level at the paddle was 0.63 m, while the depth at the toe of the cylinder (h_t) was 0.095 m. Consequently, the tests covered a wide range of limited water depth conditions ranging between $0.8 < H_o/h_t < 2.8$ (excluding non-breaking waves).

The cylinder was located at the top of a steep slope increasing from 1:20 to 1:8. Such configuration allowed the occurrence of broken impacts caused by plunging waves, which is the breaker characterized by the highest wave particle velocities.

The regular wave tests were carried out to obtain the horizontal component of the force in-line with the wave direction. To this end, two unidirectional load cells called Flexure Stainless Load Beam (FSLB) were used. The FSLB is a stainless-steel platform load cell (beam type), sealed at a waterproof level of IP67, with a nominal capacity of 890 N and an accuracy of 0.02% of the maximum capacity. Force signals were acquired at 1.8 kHz. In order to decrease resonance effects of the system, the thickness of the cylinder walls was 0.01 m and they were manufactured in Plexiglas in order to be simultaneously waterproof, rigid and light. The model was connected with two axial ball joints to the two load cells and was supported at the top by a sliding-pivot (in line with the wave direction). This support consisted of two sliding rails (circular section of low friction) and two pivots (spherical pillow blocks). The support hence avoided the weight of the model acting on the load cells. It also prevented lateral vibration due to impulsive impacts of the model whilst still allowing deflections in line with the load cell axes. Both the sliding-pivot and the load cells were attached to a framework rigidly connected to the top of the wave flume.

The frequency response of the system was empirically determined from the free oscillation of the model. It was measured both in air and with the cylindrical model slightly submerged (i.e. test condition). Results showed three dominant peaks at 25, 140 and 180 Hz. The lowest natural frequency of the system (25 Hz) ensured an accurate measurement of the force-time history for broken waves as they are typically characterized by a load impact duration larger than 0.1T.

The load cell system has the advantage of providing more accurate measurements of the overall force acting on the model than would be possible by spatially-integrated pressures. This is because pressure measurements are highly localized in both space and time [45], in part due to the aeration effect [46].

Finally, nine resistance wave gauges and three cameras completed the setup of the experiments. One camera, which was located in line with the cylindrical model (lateral side), was both high speed and high definition (3600 fps at 1024 x 1024 resolution). The other two cameras were located in different positions in order to obtain a large view, from the side and from the top, of the approaching wave. The high speed and high definition camera was used to determine breaking waves heights and the breaking distances (x) – this is the distance between the cylinder and the breaking point, which has been identified at the location where the wave starts to curl with an incipit plunging jet.

IV. Results and Discussion

The test program led to 28 fully broken impacts. These are turbulent bores characterized by relative breaking distances ($d=x/H_b$) ranging between $3.5 < d < 5.5$. Force peaks have been found to vary within a wide range. This is given by the fact that the force is affected by the combination of multiple variable, mainly:

- relative wave steepness (H_o/gT^2);
- relative wave depth (h_t/gT^2);
- relative wave height (H_o/h_t);
- relative breaking distance ($d=x/H_b$);
- aeration.

The aeration strongly affects the intrinsic random nature of the wave load typical of breaking and broken waves.

As the wave load is affected by the combination of multiple variables, no clear tendencies have been found between force peaks and one of the specific hydraulic parameters. However, maximum force peaks have been found to decrease as the time rise increases.

The wide variation in the wave load was first addressed by Bagnold [47], who noted that the impulse ($\int F\,dt$) is far more repeatable. The consistency of wave impulse has often been expressed as an exponential relationship between the maximum load peak and the time rise – time taken to get to F_{max} from 0.

In this investigation, force peaks and time rise have been analysed by means of dimensionless values. Although the development of the drag force equation in shallow water is typically dimensionless with the power of the breaking wave height (and the diameter), in this study the dimensionless force has been determined by taking into account both H_b and h_t. This is derived by the fact that the cylindrical model is located in limited water depths ($0.8 < H_o/h_t < 2.8$). Consequently, the water depth has been considered a key representative variable of the dimensionless force in this study. Therefore, dimensionless values have been obtained by dividing force peaks (F_{max}) by the specific weight of the water ($\gamma=\rho g$), breaking wave height (H_b), water depth at the toe of the cylindrical model (h_t) and average diameter of the cylinder (D); while the time rise (tr) was divided by the wave period (T).

As can be observed from Fig. 2, the dimensionless force peak (F′) has a tendency to decrease as the dimensionless impact duration (t′) increases. Dimensionless force peaks

vary between 2.1 and 0.8; while the dimensional rise time can vary between 0.12 and 0.24.

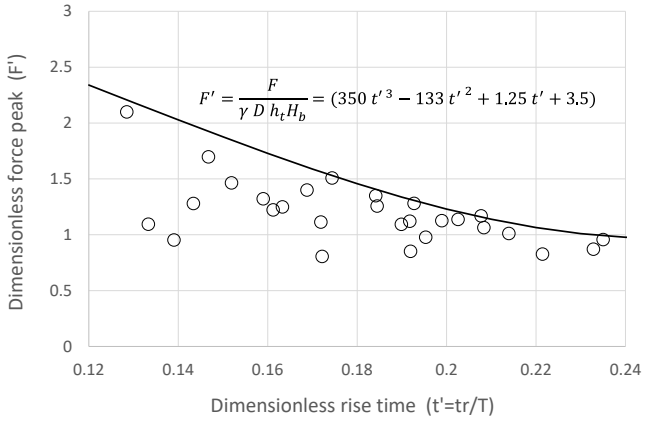

Fig. 2. Dimensionless force peak vs dimensionless rise time and envelope 3rd grade polynomial.

An envelope third grade polynomial (10) has been used to delimit maximum peak forces on the dimensionless plane force-rise time, as illustrated in Fig. 2.

$$F'(t') = \frac{F}{\gamma D\ h_t\ H_b} = (350t'^3 - 133t'^2 + 1.2t' + 3.5) \qquad (10)$$

Fig. 3 and 4 show the maximum measured force time history caused by a broken impact and its relative video frame, respectively. The hydraulic characteristics of such event, that lead to a dimensionless force peak of 2.1 (Fig. 2), are shown in Table I.

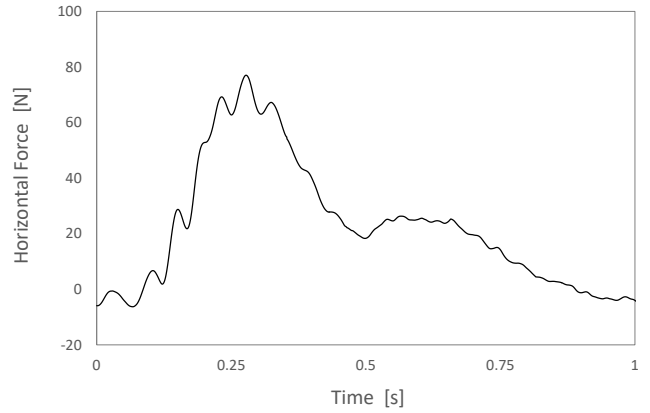

Fig. 3. Maximum measured force time history due to a broken impact.

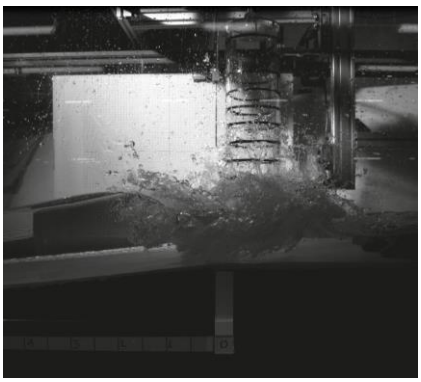

Fig. 4. Video frame related to the maximum measured force.

TABLE I
HYDRAULIC CHARACTERISTICS OF THE MAXIMUM MEASURED FORCE

$H_{o\,(target)}$ [m]	H_b [m]	T [s]
0.20	0.24	1.8

Such extreme event has been used to compare the measured force peaks with that one calculated according to the drag force of Morison equation. Fig. 5 shows the boundaries of validity of Morison equation i.e. $D/L > 0.2$. The wavelength is calculated at the toe of the cylinder (h_t=0.095 m) by means of the linear dispersion relationship (11). For the wave period T=1.8 s, the slenderness criterion is valid for both the diameters of the cylindrical model (and its average) (Fig. 5) – note that in this study broken wave impacts are characterised by wave periods T ≥ 1.2 s.

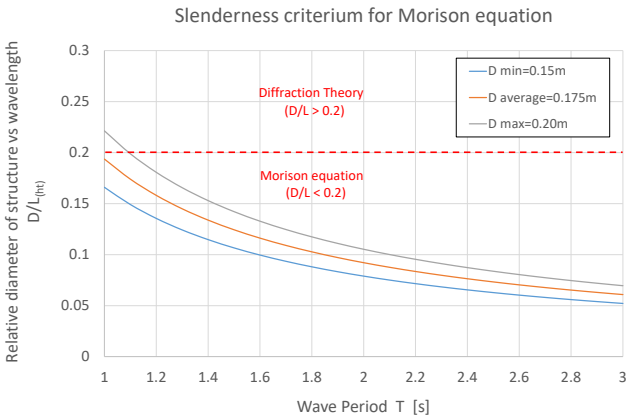

Fig. 5. Slenderness criterion for Morison equation.

$$L = \frac{g\,T^2}{2\pi}\ \tanh\left(\frac{2\,\pi\,h}{L}\right) \qquad (11)$$

As shown in (12), the drag force of Morison has been calculated by means of the values illustrated in Table II (shallow water condition).

$$F_D = 0.5\,\rho\,C_D\,D\,u\,|u|\,\Delta z = 0.5\,\rho\,C_D\,D\,g\,H_b^2 = 59\,N \qquad (12)$$

TABLE II
PARAMETERS USED TO CALCULATE MORISON FORCE

L_o	L_{ht}	h_t/L_{ht}	$u=(gH_b)^{0.5}$	$\Delta z = H_b$	C_D	KC
5.1	1.7	0.055	1.53	0.24	1.2	15.8
[m]	[m]	[-]	[m/s]	[m]	[-]	[-]

Note that:

- KC > 15: Inertia Force component of Morison equation can be neglected;
- $h_t/L(h_t) \simeq 0.05$ (shallow water): $u=C_b$ (instead of using the linear theory of Airy);
- C_D = 1.2: set at maximum value;
- D = 0.175 m (average value);
- $\Delta z = H_b \simeq$ portion hit by the turbulent bore.

Concerning the structural portion hit by the turbulent bore, two different expressions have been used in the coastal literature to delimit its impact extent i.e. $\Delta z = H_b$ or $\Delta z = (h_t + H_b/2)$. In this case, the two expressions are similar as $h_t \simeq 0.1$ and $H_b/2 \simeq 0.12$.

Based on such values, the drag force calculated with the Morison equation (59 N) results thus to be 36% smaller than the measured force (80 N) (Fig. 6). In addition, Morison equation cannot be used to estimate both the force application point and the impulse caused by broken impacts. However, these variables may play a key role in the critical dynamic response, especially when the turbine substructure is located in limited water depths and exposed to broken impacts [24]-[48]-[49]. As pointed out by the rock lighthouse investigation, spatial distributions obtained from pressure measurements were found to be characterised by extreme application points of the overall force at $1.2h_t$ from the bottom (at the instant of the force peak) [24].

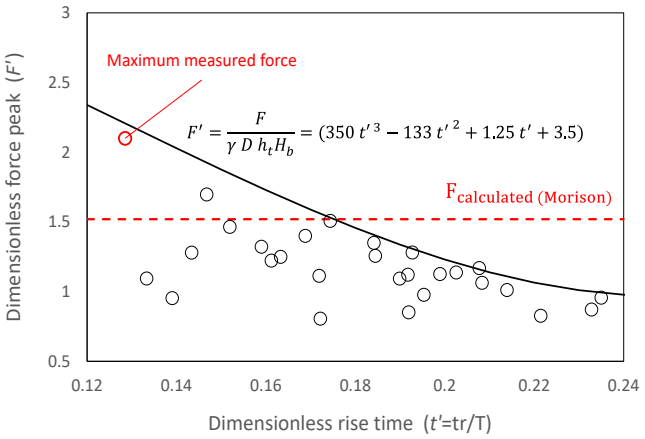

Fig. 6. Comparison between the drag force component calculated with Morison and the 3rd grade polynomial envelope.

It should be noted that the same train of supposedly identical waves (regular test) led to a wide spread of force peaks and rise time [50]. As said earlier, the high variability of the peak load is typical of breaking and broken waves, especially for the wave pressure as it is highly localized in space [45]. This is in part due to the intrinsic random nature of air-water mixture that takes place during the breaking process. In addition, the wave load is also strongly affected by small changes in wave kinematics that are influenced by previous wave train history [51].

Generally, forces obtained by load cell measurements are characterised by a smaller peak variation when compared to those measured by means of a localized pressure transducer. In this study, the force peak variation was found to be up to 30% for the same regular test. In this regard, several investigations have highlighted that critical dynamic responses may not be caused by more violent force peaks [52]. Indeed, the same impulse may lead to larger structural deflections due to the increase of the impact duration, even if it is characterised by a lower force peak [53]. Therefore, it is a good design practise to evaluate the dynamic response of turbine foundations on the basis of different impulses. As the wave load due to broken waves has an intrinsic random nature, the hydraulic conditions cannot uniquely define a force peak/rise time. Concerning this aspect, the polynomial represents an upper limit linking the maximum dimensionless force peaks due to broken impacts ($3.5 < d < 5.5$) and the dimensionless rise time – by means of four variables: H_b, h_t, T and D. Therefore, it allows estimating different impulses for the same wave condition providing, thus, a wider scenario on the critical load condition in terms of structural response. In this view, the polynomial provides 18% of scatter in terms of impulse ($I=F.2tr/2$), but a possible variation of 120% and 100% for peak force (F') and rise time (t'), respectively.

When compared to the polynomial based on the dimensionless rise time, the previous drag force of Morison results to be underestimated for values comprised between $0.12 < t' \leq 0.175$, while overestimated for $0.175 < t' < 0.25$ (Fig. 6).

V. Conclusion

A wide laboratory data set including 28 broken impacts has been analysed in order to evaluate the dynamic load acting on a cylindrical structure in limited depth conditions ranging between $0.8 < H_o/h_t < 2.8$.

The broken impacts are turbulent bores characterised by relative breaking distances between $3.5 < d = x/H_b < 5.5$. Such impacts led to a wide range of force peaks, with dimensionless values ($F' = F_{max}/\gamma H_b h_t D$) that vary between 0.8 and 2.1.

The horizontal wave force, obtained by means of load cells measurements, is affected by a combination of multiple variables (H_o/gT^2, h_t/gT^2, H_o/h_t, x/H_b, aeration). Consequently, no clear tendencies have been found between force peaks and a specific hydraulic parameter. However, maximum dimensionless force peaks (F') have been found to decrease as the dimensionless time rise ($t'=tr/T$) increases.

The maximum measured force was found to be 36% larger than the one calculated with Morison equation. Such formulation appears however to be strongly inadequate for the estimation of both the force application point and the impulse caused by broken impacts. As recently pointed out by field investigations on rock lighthouses, the structural response is strongly affected by the spatial-temporal distribution and broken impacts may represent a critical load condition when the cylindrical structure is located in limited water depths [24]. This is the case of tidal and wind turbines supported by the so-called Gravity Base Foundations, which are typically exposed to this type of load. However, no dynamic load formulations are currently available in the coastal literature to estimate the impulse due to broken waves impacting on a cylindrical structure. In this regard, an envelope 3rd grade polynomial has been developed in order to define an upper limit linking the maximum dimensionless force peaks and the

dimensionless rise time by means of four variables: H_b, h_t, T and *D*. The polynomial allows estimating different impulses for the same wave condition providing, thus, a wider scenario on the critical load condition in terms of structural response. Indeed, the same impulse may lead to larger structural deflections due to the increase of the impact duration, even if it is characterised by a lower force peak. Concerning this aspect, the polynomial provides an 18% of scatter in terms of impulse (I=F.2tr/2), but a possible variation of 120% and 100% for maximum peak force (F′) and rise time (t′), respectively.

ACKNOWLEDGEMENT

The authors would like to acknowledge Alastair Reynolds and Peter Arber for the assistance provided during the laboratory test and the School of Engineering who funded the PhD project of D. Banfi. The authors are also grateful to Emeritus Professor G. Bullock for his stimulating thoughts and for the valuable suggestions provided during the aforementioned PhD project.

REFERENCES

[1] S. Astariz, A. Vazquez, and G. Iglesias, "Evaluation and comparison of the levelized cost of tidal, wave, and offshore wind energy," *Journal of Renewable and Sustainable Energy*, 7(5), 053112, 2015.

[2] M. Buccino, D. Banfi, D. Vicinanza, M. Calabrese, G. D. Giudice, and A. Carravetta, "Non breaking wave forces at the front face of seawave slotcone generators," *Energies*, 5(11), 4779-4803, 2012.

[3] M. Buccino, D. Vicinanza, D. Salerno, D. Banfi, and M. Calabrese, "Nature and magnitude of wave loadings at Seawave Slot-cone Generators," *Ocean Engineering*, 95, 34-58, 2015.

[4] C. Perez Collazo, S. Astariz, J. Abanades, D. Greaves, and G. Iglesias, "Co-located wave and offshore wind farms: A preliminary case study of an hybrid array". *In International conference in coastal engineering (ICCE)*, 2014.

[5] F. O. Rourke, F. Boyle, and A. Reynolds, "Tidal energy update 2009," *Applied Energy*, 87(2), 398-409, 2010.

[6] C. Pérez-Collazo, D. Greaves, and G. Iglesias, "A review of combined wave and offshore wind energy," *Renewable and Sustainable Energy Reviews*, 42, 141-153, 2015.

[7] S. B. Elghali, M. E. H. Benbouzid, and J. F. Charpentier, "Marine tidal current electric power generation technology: State of the art and current status," *In Electric Machines & Drives Conference*, IEMDC'07, IEEE International, vol. 2, pp. 1407-1412, IEEE, 2007.

[8] S. Malhotra, "Selection, design and construction of offshore wind turbine foundations," *In Wind turbines*, InTech, 2011.

[9] M. Arshad, and B. C. O'Kelly, "Offshore wind-turbine structures: a review," *Proceedings of the Institution of Civil Engineers-Energy*, 166(4), 139-152, 2013.

[10] K. Y. Oh, W. Nam, M. S. Ryu, J. Y. Kim, and B. I. Epureanu, "A review of foundations of offshore wind energy convertors: Current status and future perspectives," *Renewable and Sustainable Energy Reviews*, 88, 16-36, 2018.

[11] C. A.Douglas, G. P. Harrison, and J. P. Chick, "Life cycle assessment of the Seagen marine current turbine," *Proceedings of the Institution of Mechanical Engineers, Part M: Journal of Engineering for the Maritime Environment*, 222(1), 1-12, 2008.

[12] R. J. Barthelmie, M. S. Courtney, J. Højstrup, and S. E. Larsen, "Meteorological aspects of offshore wind energy: Observations from the Vindeby wind farm," *Journal of Wind Engineering and Industrial Aerodynamics*, 62(2-3), 191-211, 1996.

[13] EWEA, "The European Offshore Wind Industry - key trends and statistics 2015," *EWEA*, Technical report, 2016.

[14] M. Achmus, Y. S. Kuo, and K. Abdel-Rahman, "Behavior of monopile foundations under cyclic lateral load," *Computers and Geotechnics*, 36(5), 725-735, 2009.

[15] J. Abanades, J. Ivars, R. Molina, and C. García, "The Application of Caisson-Type Solutions to the Current Offshore Wind Energy Market," *In ASME 2018 37th International Conference on Ocean, Offshore and Arctic Engineering, American Society of Mechanical Engineers*, 2018.

[16] M. van Wijngaarden, "Gravity based foundations for offshore wind turbines: Cyclic loading and liquefaction," Master thesis in Hydraulic Engineering, Delft University of Technology, Netherlands, 2018.

[17] I. Ruiz de Temiño Alonso, "Gravity base foundations for offshore wind farms: marine operations and installation processes," Master thesis in European Construction Engineering, University of Cantabria, Spain, 2013.

[18] R. Dahlberg, "Observations of scour around offshore structures," *Canadian geotechnical journal*, 20(4), 617-628, 1983.

[19] R. J. Whitehouse, J. Sutherland, and J. Harris, "Evaluating scour at marine gravity foundations," *Proceedings of the ICE-Maritime Engineering*, 164(4), 143-157, 2011.

[20] R. T. Koekkoek, "Gravity base foundations for offshore wind turbines," Master thesis in Civil Engineering, Delft University of Technology, Netherlands, 2015.

[21] J. Morison, J. Johnson, and S. Schaaf, "The force exerted by surface waves on piles," *Journal of Petroleum Technology*, 2(05), 149-154, 1950.

[22] DNV, Det Norske Veritas. "Design of offshore wind turbine structures." Standard DNV-OSJ101, Det Norske Veritas AS (DNV), 2013.

[23] R. Manjula, S. A. Sannasiraj, and K. Palanichamy, "Experimental Investigations of acceleration on slender cylindrical member under breaking waves," *The International Journal of Ocean and Climate Systems*, 5(3), 117-125, 2014.

[24] D. Banfi, "A field and laboratory study on the dynamic response of the Eddystone lighthouse to wave loading," Ph.D. dissertation, University of Plymouth, UK, 2018.

[25] C. J. Galvin Jr, "Breaker type classification on three laboratory beaches," *Journal of geophysical research*, 73(12), 3651-3659, 1968.

[26] K. Tanimoto, S. Takahashi, T. Kaneko, and K. Shiota, "Impulsive breaking wave forces on an inclined pile exerted by random waves," *In Coastal Engineering 1986*, pp. 2288-2302, 1987.

[27] D. Zhou, E. S. Chan, and W. K. Melville, "Wave impact pressures on vertical cylinders," *Applied Ocean Research*, 13(5), 220-234, 1991.

[28] E. S. Chan, and W. K. Melville, "Plunging wave forces on surface-piercing structures," J*ournal of Offshore Mechanics and Arctic Engineering*, 111(2), 92-100, 1989.

[29] H. Bredmose, and N. G. Jacobsen, "Breaking wave impacts on offshore wind turbine foundations: focused wave groups and CFD," *In ASME 2010 29th International Conference on Ocean, Offshore and Arctic Engineering, American Society of Mechanical Engineers*, pp. 397-404, 2010.

[30] S. Schløer, H. Bredmose, and R. F. Mikkelsen, "Fatigue and extreme wave loads on bottom fixed offshore wind turbines. Effects from fully nonlinear wave forcing on the structural dynamics," 2013.

[31] S. Schløer, H. Bredmose, and A. Ghadirian, "Analysis of experimental data: The average shape of extreme wave forces on monopile foundations and the NewForce model," *Energy Procedia*, 137, 223-237, 2017.

[32] E.D. Christensen, E.A. Hansen, L. Yde, N.J. Tarp-Johansen, H. Gravesen, and M.L. Damsgaard, "Wave loads on offshore wind turbine foundations in shallow water: engineering models vs. refined flow modelling," *In Proceedings of the European Offshore Wind Conference*, pp. 4-6, 2007.

[33] M. A. Chella, A. Tørum, and D. Myrhaug, "An overview of wave impact forces on offshore wind turbine substructures," *Energy Procedia*, 20, 217-226, 2012.

[34] O. T. Gudmestad, and G. Moe, "Hydrodynamic coefficients for calculation of hydrodynamic loads on offshore truss structures," *Marine Structures*, 9(8), 745-758, 1996.

[35] E. R. Johnson, "Horizontal forces due to waves acting on large vertical cylinders in deep water," *Journal of Basic Engineering*, 94(4), 862-866, 1972.

[36] M. Arshad, and B.C. O'Kelly, "Analysis and design of monopile foundations for offshore wind-turbine structures," *Marine Georesources & Geotechnology*, 34(6), 503-525, 2016.

[37] J. R. Chaplin, T. Flintham, C. Greated, and D. Skyner, "Breaking wave forces on a vertical cylinder," Health and Safety Executive, London, Technical Report No. OTH, 90, 324, 1992.

[38] H. Bredmose, J. Skourup, E.A. Hansen, E. D. Christensen, L. M. Pedersen, and A. Mitzlaff, "Numerical reproduction of extreme wave loads on a gravity wind turbine foundation," *In 25th International Conference on Offshore Mechanics and Arctic Engineering, American Society of Mechanical Engineers*, pp. 279-287, 2006.

[39] A. Ghadirian, and H. Bredmose, "Initial experimental validation of a pressure impulse model for a vertical cylinder," presented at the *Int. Workshop of Water Waves & Floating Bodies*, 2019.

[40] J. Wienke, and H. Oumeraci, "Breaking wave impact force on a vertical and inclined slender pile —theoretical and large-scale model investigations," *Coastal Engineering*, 52(5), 435-462, 2005.

[41] B. T. Paulsen, B. de Sonneville, M. van der Meulen, and N. G. Jacobsen, "Probability of wave slamming and the magnitude of slamming loads on offshore wind turbine foundations," *Coastal Engineering*, 143, pp. 76-95, 2018.

[42] A. Raby, G. N. Bullock, D. Banfi, Y. Rafiq, and F. Cali, "Wave loading on rock lighthouses," *In Proceedings of the Institution of Civil Engineers-Maritime Engineering*, vol. 169, no. 1, pp. 15-28, Thomas Telford Ltd, 2015.

[43] E. D. Christensen, H. Bredmose, and E.A. Hansen, "Extreme wave forces and wave run-up on offshore wind turbine foundations," *Proceedings of Copenhagen Offshore Wind*, 1-10, 2005.

[44] T. L. Andersen, P. Frigaard, M. L. Damsgaard, and L. De Vos, "Wave run-up on slender piles in design conditions — Model tests and design rules for offshore wind," *Coastal Engineering*, 58(4), 281-289, 2011.

[45] G. N. Bullock, C. Obhrai, D. H. Peregrine, and H. Bredmose, "Violent breaking wave impacts. Part 1: Results from large-scale regular wave tests on vertical and sloping walls," *Coastal Engineering*, 54(8), 602-617, 2007.

[46] G. N. Bullock, A. R. Crawford, P. J. Hewson, M. Walkden, and P. A. D Bird, "The influence of air and scale on wave impact pressures," *Coastal Engineering*, 42(4), 291-312, 2011.

[47] R. A. Bagnold, "Interim report on wave-pressure research," Excerpt from the J. of the Institution of Civil Engineers, 1939.

[48] M. Muttray, H. Oumeraci, K. Shimosako, and S. Takahashi, "Hydraulic performance of a high mound composite breakwater," *In Coastal Engineering 1998*, pp. 2207-2220, 1999.

[49] Q. Trinh, A. Raby, D. Banfi, M. Corrado, B. Chiaia, Y. Rafiq, and F. Cali, "Modelling the Eddystone Lighthouse response to wave loading," *Engineering Structures*, 125, 566-578, 2016.

[50] G. Cuomo, R. Piscopia, and W. Allsop, "Evaluation of wave impact loads on caisson breakwaters based on joint probability of impact maxima and rise times," *Coastal Engineering*, 58(1), 9-27, 2011.

[51] G. N. Bullock, P. K. Stansby, and J. G. Warren, J. G. "Loading and response of cylinders in waves," *In Coastal Engineering 1978*, pp. 2415-2432, 1978.

[52] R. Manjula, S. A. Sannasiraj, and K. Palanichamy, K. "Experimental Investigations of acceleration on slender cylindrical member under breaking waves," *The International Journal of Ocean and Climate Systems*, 5(3), 117-125, 2014.

[53] C. Loraux, "Comportement structural des phares en mer étude historique sur le phare de la Jument et propositions d'interventions," Master thesis, Institut D'Ingénierie Civile, École Polytechnique Fédérale De Lausanne, France, 2013.